Fate of the false Mott-Hubbard transition in two dimensions

T. Schäfer,[1] F. Geles,[2] D. Rost,[3,4] G. Rohringer,[1] E. Arrigoni,[2] K. Held,[1] N. Blümer,[3] M. Aichhorn,[2] and A. Toschi[1]

[1]*Institute of Solid State Physics, Vienna University of Technology, 1040 Vienna, Austria*

[2]*Institute of Theoretical and Computational Physics, Graz University of Technology, Graz, Austria*

[3]*Institute of Physics, Johannes Gutenberg University, Mainz, Germany*

[4]*Graduate School Materials Science in Mainz, Johannes Gutenberg University, Mainz, Germany*

(Received 13 June 2014; revised manuscript received 10 February 2015; published 3 March 2015)

We have studied the impact of nonlocal electronic correlations at all length scales on the Mott-Hubbard metal-insulator transition in the unfrustrated two-dimensional Hubbard model. Combining dynamical vertex approximation, lattice quantum Monte Carlo, and variational cluster approximation, we demonstrate that scattering at long-range fluctuations, i.e., Slater-like paramagnons, opens a spectral gap at weak-to-intermediate coupling, irrespective of the preformation of localized or short-range magnetic moments. This is the reason why the two-dimensional Hubbard model has a paramagnetic phase which is insulating at low enough temperatures for any (finite) interaction and no Mott-Hubbard transition is observed.

DOI: 10.1103/PhysRevB.91.125109 PACS number(s): 71.27.+a, 71.10.Fd, 71.30.+h

I. INTRODUCTION

The Mott-Hubbard metal-insulator transition (MIT) [1] is one of the most fundamental hallmarks of the physics of electronic correlations. Nonetheless, astonishingly little is known exactly, even for its simplest modeling, i.e., the single-band Hubbard Hamiltonian [2]: Exact solutions for this model are available only in the extreme, limiting cases of one and infinite dimensions.

In one dimension, the Bethe ansatz shows that there is actually no Mott-Hubbard transition [3–5]; in other words, it occurs for a vanishingly small Hubbard interaction U. At any $U > 0$ the one-dimensional (1D) Hubbard model is insulating at half filling. One dimension is, however, rather peculiar: While there is no antiferromagnetic ordering even at temperature $T = 0$, antiferromagnetic spin fluctuations are strong and long ranged, decaying slowly, i.e., algebraically. Also, the (doped) metallic phase is not a standard Fermi liquid but a Luttinger liquid.

For the opposite extreme, infinite dimensions, the dynamical mean-field theory (DMFT) [6] becomes exact [7], which allows for a clear-cut and, to a certain extent, almost "idealized" description of a pure Mott-Hubbard MIT. In fact, since in $D=\infty$ only local correlations survive [7], the Mott-Hubbard insulator of DMFT consists of a collection of localized (but not long-range ordered) magnetic moments. This way, if antiferromagnetic order is neglected or sufficiently suppressed, DMFT describes a first-order MIT [6,8], ending with a critical end point.

As an approximation, DMFT is applicable to the more realistic cases of the three- and two-dimensional Hubbard models. However, the DMFT description of the MIT is the very same here since only the noninteracting density of states (DOS) and, in particular, its second moment enter. This is a natural shortcoming of the mean-field nature of DMFT: antiferromagnetic fluctuations have *no* effect at all on the DMFT spectral function or self-energy above the antiferromagnetic ordering temperature T_N.

In three dimensions, antiferromagnetic fluctuations reduce T_N sizably compared to the DMFT (see Fig. 1), although they are significant only at $T \simeq T_N$. Hence, the reliability of the DMFT results for the spectral functions is not spoiled in three dimensions except for the proximity of the antiferromagnetic transition [9–12], whereas deviations from the DMFT entropy and susceptibilities can be significant also at higher T [12,13]. With this background, it is maybe not surprising that DMFT also yields a good description of the MIT even for realistic material cases, such as the textbook example V_2O_3 [14].

Much more intriguing, and challenging, is the two-dimensional (2D) case, which is most relevant for high-temperature superconductivity and the rapidly emerging field of oxide thin films and heterostructures. In fact, this issue has been intensely debated since the 1970s: On the one hand, several analytical and numerical results [15–20] suggested that a metallic phase is found at weak coupling, with a MIT at a finite U_c. At the same time, calculations with the two-particle self-consistent (TPSC) approach [21–23] showed a pseudogap in the perturbative regime of small U [24]. Finally, in Anderson's view [25] the 2D physics should be considered fully nonperturbative, similar [5] to that in one dimension, yielding a Mott gap and the localized physics of the 2D Heisenberg Hamiltonian for all $U > 0$.

More recently, most precise numerical studies have shown unambiguously that the short-range spin fluctuations do actually reduce the critical interaction U_c for the MIT in two dimensions compared to DMFT *and* reverse its slope (see Fig. 1). (Note that the DMFT insulating phase has the full entropy of free spins, i.e., $\ln 2$ per site, implying the positive DMFT slope $dU_c/dT > 0$ of Fig. 1.) Such a 2D picture has been established by cluster DMFT (CDMFT) [26], dynamical cluster approximation (DCA) [27,28], and second-order dual-fermion [29] studies [30], which systematically include nonlocal correlations beyond DMFT. However, given the limited cluster sizes of CDMFT and DCA calculations, only short-range correlations are included.

In this paper, we revisit the MIT in two dimensions and the effect of antiferromagnetic spin-fluctuations thereupon. To this end, we employ three methods: (i) the variational cluster approximation (VCA) [31], which includes short-range correlations, (ii) the dynamical vertex approximation (DΓA), which includes short- *and* long-range correlations beyond DMFT on the same footing [32], and (iii) lattice quantum Monte Carlo (QMC) simulations [33–35] of unprecedented accuracy

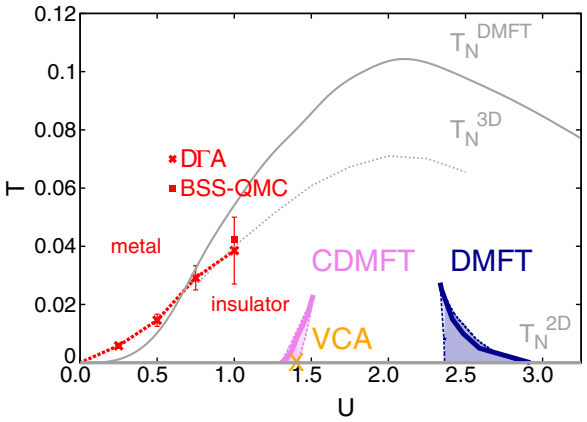

FIG. 1. (Color online) MIT of the Hubbard model on a square lattice determined by different nonperturbative techniques. The DMFT transition line (blue [39]) is shifted towards lower interaction values due to short-range spatial correlations (violet line: CDMFT [26]; orange cross at $T = 0$: VCA). This trend is accompanied by a simultaneous shrinking of the coexistence regions (hatched regions). The inclusion of long-range fluctuations leads to a vanishing U_c in the low-temperature regime (crosses and red dashed line: DΓA; solid red box: BSS-QMC). Error bars mark the temperature range, where the onset of an insulating behavior on the whole Fermi surface has been found, according to the electronic self-energy of DΓA (see Fig. 3). Also shown are the DMFT [9] and the DΓA 3D Néel temperatures (light gray dotted lines) [11] as well as the DΓA 2D one (gray line at $T = 0$) [40] which fulfills the Mermin-Wagner theorem [41]; $4t \equiv 1$ sets the energy scale.

made possible by the algorithmic progress, increased computer power, and careful extrapolations (see the Appendix) [36,37].

II. PHASE DIAGRAM IN TWO DIMENSIONS

Let us first summarize the results of our combined comparative studies for the half-filled Hubbard model on a square lattice with nearest-neighbor hopping $t \equiv 1/4$ using the phase diagram in Fig. 1; all details on the spectra and the underlying physics of the different regimes are presented afterwards.

Our VCA data for the MIT at zero temperature (orange cross in Fig. 1) appear to be consistent with the previous CDMFT, DCA, and older VCA [38] studies, as well as with second-order dual-fermion [29] calculations [30]: short-range antiferromagnetic correlations reduce the critical U_c (violet line) significantly with respect to DMFT. Moreover, the width of the coexistence region is considerably reduced (see the violet hatched area for CDMFT [26]). The VCA calculations performed on different clusters, however, also suggest something more definite in this respect: At low temperatures, the smaller U is, the more important the effect of longer-range antiferromagnetic fluctuations becomes.

To address this issue in more detail, we include such long-range correlations by means of DΓA. Results are also compared with lattice Blankenbecler-Scalapino-Sugar (BSS) QMC calculations [33]. The red dashed line in Fig. 1 marks the interaction $U_c(T)$, above which, for a given temperature T, a spectral gap is opened because of a strong enhancement of the electronic scattering rate in the very low frequency regime (see below).

These DΓA data, confirmed by our extrapolated BSS-QMC data, strongly suggest that at low enough T strong antiferromagnetic spin fluctuations *always* open a spectral gap, even at arbitrarily small values of U (red dashed line in Fig. 1). Hence, for $T \to 0$, $U_c \to 0$; that is, *no* MIT can be identified any longer for the 2D unfrustrated Hubbard model, similar to what happens in one dimension. As we will elaborate in the following, the mechanism is, however, rather different in this case. By increasing U the temperature of the onset of the insulating behavior is enhanced until the high-temperature crossover regime of DMFT at intermediate U is reached: Here, the electron mobility is already suppressed by purely local correlations.

Our results for the phase diagram indicate that the "idealized" physical picture of the Mott-Hubbard metal-insulator transition of DMFT is completely overturned in two dimensions by strong, spatially extended antiferromagnetic correlations. In the following, we will discuss explicitly the most important aspects in terms of spatial correlations over different length scales and their underlying physics by analyzing in detail the numerical data used for determining the phase diagram in two dimensions.

III. SHORT-RANGE CORRELATIONS

The physics of short-range correlations at $T = 0$ is captured very well by VCA in the paramagnetic phase. In fact, our results for a VCA cluster of $N_c = 4$ sites (plus four bath sites) show a clear-cut MIT at a finite $U_c = 1.4$ for $T = 0$, within the CDMFT coexistence region of a metallic and an insulating solution. The local spectral function $A(\omega)$ and the self-energy $\Sigma(i\omega_n)$ at the Fermi level of the two coexisting solutions at $U = U_c = 1.4$ are reported in Fig. 2. The two solutions differ qualitatively, showing a correlated metallic behavior with a quasiparticle weight of $Z_{\mathrm{VCA}} = 0.37$ at $\mathbf{k} = (\pi,0)$ (bottom panel) and an insulating behavior (top panel) characterized by a divergence of Im $\Sigma(i\omega_n)$ and a corresponding spectral gap, respectively. The VCA calculation of the grand potential indicates that for $U < U_c = 1.4$ the thermodynamically stable solution is the metallic one, while for $U > 1.4$ the insulator is stabilized, with a level crossing at $U = U_c$. Such a U_c value is in fairly good agreement with CDMFT [26]; it gets reduced by slightly increasing the lattice size in the VCA calculations from $U_c = 1.4$ for $N_c = 4 = 2 \times 2$ to $U_c = 1.325$ for $N_c = 6 = 2 \times 3$. This reflects the fact that correlations of very short range (actually two sites in the case of $N_c = 4$) are strong enough to destroy the low-temperature metallic phase at intermediate coupling but are less effective for lower values of the interaction. In fact, in the presence of a $T = 0$ (magnetic) instability, a correct description of the weak-coupling regime in two dimensions cannot be obtained without the inclusion of correlations on *all* length scales, as we show in the following.

IV. LONG-RANGE CORRELATIONS

We include correlations on all length scales by either extrapolating lattice BSS-QMC results to $N_c \to \infty$ or using DΓA [32] in its ladder version [40], a diagrammatic extension

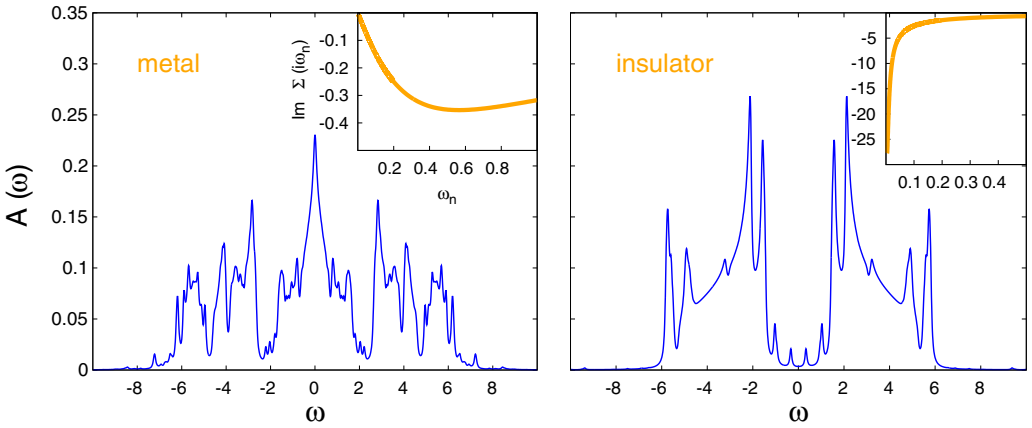

FIG. 2. (Color online) Local spectral function of the two coexisting solutions obtained in VCA at the $T = 0$, $U = U_c = 1.4$ MIT for a four-site cluster plus four bath sites. (left) Metallic solution; (right) insulating solution. The insets show the corresponding self-energies at $\mathbf{k} = (\pi,0)$.

of DMFT (see [29,42,43]) based on the two-particle vertex [44,45]. Certainly, both approaches have their limitations, either due to the extrapolation procedure of the cluster results (see the Appendix) or due to the selection of the more relevant subsets of diagrams. Hence, cross-checking the results of these complementary approaches, as we do here, is of utmost importance. In fact, the good agreement observed (top panels of Fig. 3) validates our results and at the same time supports the physical interpretation discussed below. The top panels of Fig. 3 show our DΓA and BSS-QMC data of the imaginary part of the electronic self-energy $\Sigma(\mathbf{k},i\omega_n)$ for the most significant $\mathbf{k}$ points at the Fermi surface [i.e., the "nodal" point $\mathbf{k} = (\frac{\pi}{2},\frac{\pi}{2})$ and the "antinodal" point $\mathbf{k} = (\pi,0)$] as a function of Matsubara frequencies for a rather small value of $U = 0.5$ at two different temperatures ($T = 0.025$ and $T = 0.010$). Here, one can immediately appreciate how the one-particle physics changes even qualitatively when reducing T: At $T = 0.025$ both DΓA (top left panel) and lattice QMC (left inset) self-energies display a Fermi-liquid behavior for all $\mathbf{k}$ points, not radically different from the DMFT results (blue squares in Fig. 3). Even the quasiparticle renormalization $Z = (1 - \frac{\partial \mathrm{Im}\Sigma(\mathbf{k},i\omega_n)}{\partial\omega_n}|_{\omega_n\to 0})^{-1} \simeq 0.9$ is similar. In contrast, the scattering rate γ at the Fermi surface is increased from $\gamma_{\mathrm{DMFT}} = -\mathrm{Im}\Sigma_{\mathrm{DMFT}}(\mathbf{k},i0^+) = 0.002$ to ($\mathbf{k}$ averaged) $\bar{\gamma}_{D\Gamma A} \simeq 0.014$, with a moderate $\mathbf{k}$ differentiation [46]. By reducing T, $\gamma_{D\Gamma A}$ quickly gets enhanced on the whole Fermi surface, always displaying its largest value at $\mathbf{k} = (\pi,0)$. At $T = 0.010$ the self-energy has already changed completely (see Fig. 3, right): $\mathrm{Im}\Sigma(\mathbf{k},i\omega_n)$ acquires an evident downturn for all $\mathbf{k}$ points at very low frequencies. This shows that the Fermi surface is completely destroyed at low T, even at the nodal momentum $\mathbf{k} = (\pi/2,\pi/2)$. Such a qualitative change in the low-frequency self-energy behavior has been exploited for defining the red dashed line marking the destruction of the whole Fermi surface and hence insulating behavior in our phase diagram (Fig. 1).

V. PHYSICAL INTERPRETATION

Our combined numerical analysis shows that there is no Mott-Hubbard transition at finite U in the unfrustrated 2D Hubbard model, but it also clarifies unambiguously the physical origin of this result. Evidently, the shift of the border of the MIT towards $U = 0$ (Fig. 1) already represents an indication for rather extended spatial fluctuations, which emerge from the proximity to the $T = 0$ long-range antiferromagnetic order. The important questions still to be answered are, Can this intuitive picture be confirmed in a less heuristic and more direct way? What is the exact nature of these extended antiferromagnetic spin fluctuations? These questions can be answered by extending our study of the low-T weak-coupling regime to the DΓA spin-correlation function $\chi_s(\mathbf{r},i\Omega_n = 0) = \int_0^\beta d\tau \langle S_z(\mathbf{r},\tau)S_z(0,0)\rangle$ in real space. Our results for $U = 0.5$ are reported in the middle panels of Fig. 3, where we show, as a representative case, the spatial decay of χ_s along the x direction, normalized to its $\mathbf{r} = 0$ value at $T = 0.025$ (metal) and $T = 0.010$ (insulator): In both cases, χ_s displays an alternating sign, which is the typical hallmark of predominant antiferromagnetic fluctuations. The spatial extensions of such fluctuations are quite different, however. In fact, the long-distance behavior of χ_s can be approximated by its asymptotic expression $|\chi_s(r\to\infty)| \propto \sqrt{\frac{\xi}{r}}\, e^{-r/\xi}$ [47]. But the correlation length ξ varies from ~ 4 in the metallic phase to values of $\xi \approx 1000$ in the low-T insulating phase. A more quantitative understanding is provided by the study of the T dependence of ξ in DΓA (see bottom panels of Fig. 3). By reducing T, ξ displays a well-defined crossover to an exponential behavior, which approximately matches the onset of the low-T insulating regime at weak coupling. This shows that the spin fluctuations responsible for the destruction of the Fermi surface at low T have such a large spatial extension that it is difficult to capture with (nonextrapolated) cluster calculations [48,49]. For instance, the corresponding VCA self-energy at $T = 0$ (orange curve in Fig. 3) displays a very clear metallic behavior, similar to that of DMFT.

Insight can also be gained from the potential energy. Our DΓA and BSS-QMC results show that the destruction of the metallic state upon decreasing T is accompanied by a slight reduction in potential energy $U\langle n_\uparrow n_\downarrow\rangle$ by about 1% for the data in Fig. 3. However, this effect occurs in the presence of strong and very extended ($\xi \gg 100$) spin correlations.

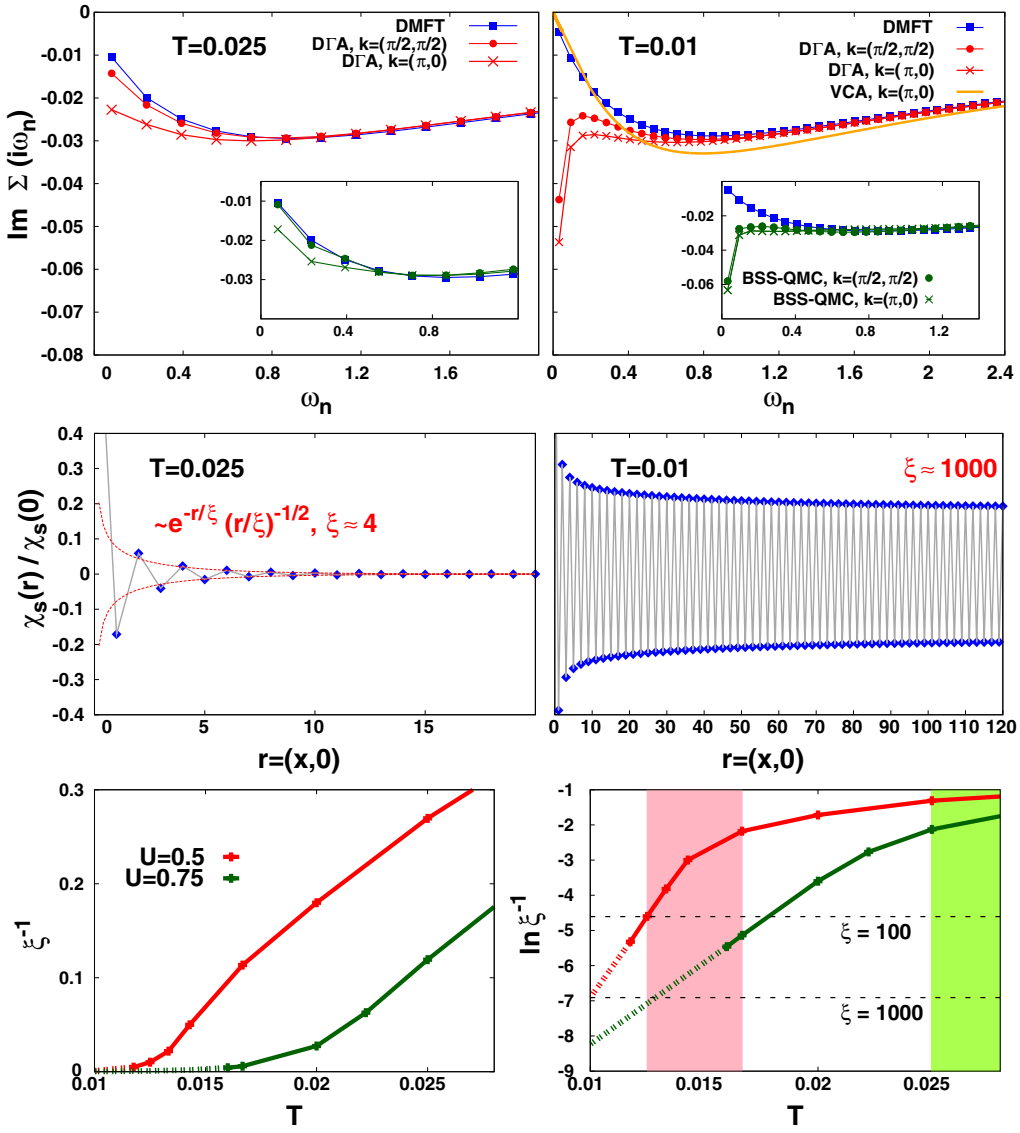

FIG. 3. (Color online) (top) Imaginary parts of the self-energies for $U = 0.5$ and $T = 0.025$ (left) and $T = 0.010$ (right), comparing DMFT (blue squares), DΓA [red circles: $\mathbf{k} = (\pi/2,\pi/2)$; red crosses: $\mathbf{k} = (\pi,0)$], VCA (orange; $T = 0$), and BSS-QMC (insets; see the Appendix). Even for the very small interaction $U = 0.5$ an insulating gap is opened at $T \approx 0.014$ in DΓA as well as in BSS-QMC. (middle) Real-space dependence of the DΓA spin-correlation function $\chi_s(\mathbf{r})/\chi_s(\vec{0})$ for the same parameters as above. Shown is the cut $\mathbf{r} = (x,0)$, where x is given in units of the lattice spacing $a = 1$. The solid gray line (guide to the eye) interpolates between the values at different lattice vectors (blue diamonds). By fitting (see also the dashed lines in the bottom panels) we obtain the correlation lengths $\xi \approx 4$ at $T = 0.025$ (left), while $\xi \approx 1000$ at $T = 0.010$ (right). (bottom) T dependence of ξ^{-1} for different interaction values. A crossover to an exponential behavior is observed at T consistent with the onset of the insulating behavior [pink (green) area for $U = 0.5$ (0.75)].

Therefore, the physics cannot be really different from the truly long-range ordered phase [50]. This rules out any particular role of prelocalization of the magnetic moments in destroying the Fermi-liquid state, as well as the possibility of mapping the whole low-T physics onto the 2D Heisenberg model, as proposed by Anderson [25]. Rather, the emerging physics appears to be more consistent with the description of the TPSC approach [22,23], at least in the weak-coupling regime, and of the low-T calculations with the nonlinear sigma model [51], as well as to the experimental estimates of ξ in electron-doped cuprates [52]. In fact, the slight decrease in the potential energy is a clear hallmark [53–55] of the Slater-like nature of the antiferromagnetic fluctuations as is the large ξ. We can hence interpret this as "Slater paramagnons." The corresponding physical picture is the following: For all $U > 0$, a gap is opened at low enough T because of the enhanced electronic scattering with extended antiferromagnetic paramagnons. The nature of such spin fluctuations, reflecting the behavior of the $T = 0$ ordered phase [51,56] from which they originate, smoothly evolves from Slater (weak to intermediate coupling) to Heisenberg (strong coupling). In this respect, it is worth recalling that DCA results [53] on small clusters ($N_c = 4$) also suggest the crossover from Slater-like to Heisenberg-like fluctuations for U larger than (at least) 1.25. Although still smaller [48], these interaction values are not too far away from the regime where the crossover to Heisenberg physics

is predicted to occur in the long-range ordered phase by DMFT [54].

VI. CONCLUSIONS

We have studied the effects of spatial correlations on different length scales on the MIT in the 2D half-filled Hubbard model: for all $U > 0$, at low enough (but finite) T, we find a paramagnetic insulator. This is the result of strong scattering at extended antiferromagnetic fluctuations (paramagnons). The nature of these fluctuations gradually evolves from Slater-like to Heisenberg-like, tracking an analogous evolution for the $T = 0$ antiferromagnet. This physical picture is quite different from both state-of-the art DMFT/CDMFT, which finds a finite U_c for the (metastable) paramagnetic phase, and the strong-coupling idea of an effective low-T 2D Heisenberg model, which assumes preformed spins even at low U. Instead, the 2D Hubbard model has $U_c = 0$, and the nature of the most relevant spin fluctuations is Slater-like in the whole weak- to intermediate-coupling regime. Let us stress that if we frustrate the 2D square lattice away from perfect nesting, e.g., by adding a nearest-neighbor hopping, antiferromagnetism and hence the MIT originating from antiferromagnetic fluctuations are expected to shift to a finite $U_c > 0$, implying a quantum critical point.

ACKNOWLEDGMENTS

We thank S. Andergassen, M. Capone, M. Fabrizio, E. Gull, O. Gunnarsson, H. Hafermann, J. Le Blanc, A. Katanin, C. Taranto, and A. Valli for discussions. We acknowledge support from the Austrian Science Fund (FWF) through the Doctoral School "Building Solids for Function" (T.S.; FWF project ID W1243), SFB ViCoM (E.A., F.G., K.H., M.A., A.T.; FWF project ID F4103), and NAWI Graz; from the research unit FOR 1346 and the graduate school GSC 266 of the German Research Foundation (DFG) (DR,NB). Calculations were performed on the Vienna Scientific Cluster (VSC).

APPENDIX

The numerical results presented in this paper have been obtained using complementary techniques with quite different characteristics. Among those, the dynamical vertex approximation (DΓA) yields results directly in the thermodynamic limit [32]; the variational cluster approximation (VCA), on the other hand, is good for short-range correlations [31], and finally, the Blankenbecler-Scalapino-Sugar (BSS) QMC calculations for the Hubbard model are applicable to clusters with a finite number N of lattice sites, with $N = L^2$ for square lattices with linear extent L. In its generic formulation, the BSS-QMC algorithm introduces a further systematic bias due to a Trotter discretization of the imaginary time [33]. In this work, we employ a multigrid approach for obtaining quasicontinuous imaginary-time Green's functions without significant Trotter bias [37], which can be reliably Fourier transformed in order to compute self-energies; similar strategies have proven successful in the context of DMFT studies using the Hirsch-Fye QMC algorithm [36,57,58]. As a result, all "raw" data shown in this appendix should be regarded as numerically exact for a given cluster size. The BSS-QMC computational effort scales as N^3/T at temperature T, i.e., proportionally to L^6 at fixed T, which limits high-precision calculations (as we need here for determining the self-energy on the percent level) to $L \lesssim 16$. The properties of such finite systems will, in general, depend on the exact system size (and shape as well as boundary conditions) and may deviate drastically from the thermodynamic limit.

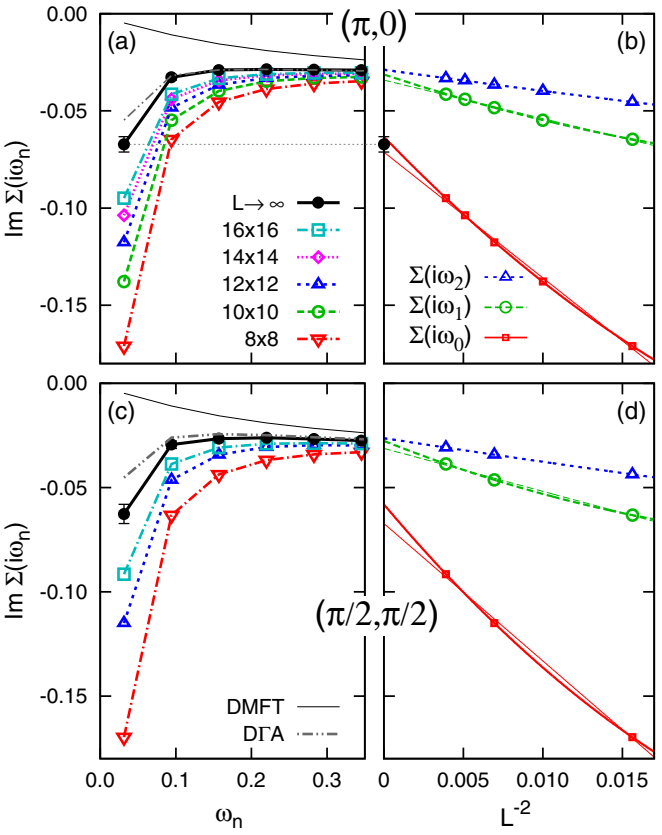

FIG. 4. (Color online) Self-energy on the imaginary axis at $U = 0.5$, $\beta = 100$. (a) Finite-size BSS-QMC data (open symbols and colored lines), extrapolated BSS-QMC results in the thermodynamic limit (circles and thick black solid line), and DΓA data (gray dash-double-dotted line) vs Matsubara frequency ω_n at momentum $\mathbf{k} = (\pi,0)$; also shown are momentum-independent single-site DMFT results (thin black line). (b) Finite-size BSS-QMC (symbols) data for the first three Matsubara frequencies vs inverse system size plus extrapolations in linear order in L^{-2} (thin lines) and quadratic order (thick lines). (c) and (d) Analogous analysis at $\mathbf{k} = (\pi/2,\pi/2)$.

We will show in the following that reliable extrapolations to the thermodynamic limit, as shown in Fig. 3, are still possible in the parameter range of interest based on BSS-QMC data obtained for quadratic clusters (with periodic boundary conditions) and linear extents $L = 8,10,12,14,16$.

In the left column of Fig. 4, estimates of the self-energy $\Sigma(\mathbf{k},i\omega_n)$ at interaction $U = 0.5$ and inverse temperature $\beta = 100$ are shown versus Matsubara frequency ω_n for the two momenta $\mathbf{k} = (\pi,0)$ [Fig. 4(a)] and $\mathbf{k} = (\pi/2,\pi/2)$ [Fig. 4(c)]; due to particle-hole symmetry the self-energy is purely imaginary at these $\mathbf{k}$ points. Finite-size (FS) BSS-QMC data

(open symbols and colored lines) depend strongly on the lattice size: with decreasing linear extent L, they show increasingly insulating tendencies, i.e., larger absolute values of Im $\Sigma(i\omega_n)$ at the lowest ω_n. However, as demonstrated in Fig. 4(b), for the lowest three Matsubara frequencies at $\mathbf{k} = (\pi,0)$, this bias is very systematic: Already linear extrapolations in the inverse size L^{-2} (thin solid lines) yield reasonable first estimates of the thermodynamic limit $L^{-2} \to 0$. Much better fits can be obtained at higher orders, e.g., using quadratic fits in L^{-2} (thick lines); however, these become increasingly unstable (in the presence of statistical noise) at higher orders. In order to define a consistent procedure that is also stable at $\mathbf{k} = (\pi/2,\pi/2)$, where fewer system sizes are available (see below), we use the average of linear and quadratic extrapolation as the final result, with error bars that coincide with the individual extrapolations, as illustrated by the black circle with error bars for $\Sigma(i\omega_0)$ in Fig. 4(b):

$$\Sigma^{\infty} = \tfrac{1}{2}\left(\Sigma^{\infty}_{\text{lin}} + \Sigma^{\infty}_{\text{quad}}\right), \quad \Delta\Sigma^{\infty} = \tfrac{1}{2}\left|\Sigma^{\infty}_{\text{lin}} - \Sigma^{\infty}_{\text{quad}}\right|.$$

The final result of this extrapolation [black circles in Fig. 4(a)] shows perfect agreement with DΓA (gray dash-double-dotted line) at almost all Matsubara frequencies. A minor quantitative deviation is only observed at the smallest Matsubara frequency, at which the absolute value of $\text{Im}\Sigma(\mathbf{k},\omega)$ is somewhat smaller in DΓA.

Since only lattices with linear dimensions $L = 4,8,12,\ldots$ contain the momentum $\mathbf{k} = (\pi/2,\pi/2)$ in the Brillouin zone (for periodic boundary conditions), we have only three system sizes available for extrapolation in this case [symbols in Fig. 4(d)]. However, the curvatures of the (here, necessarily perfect but intrinsically somewhat unstable) quadratic fits agree well with those obtained at $\mathbf{k} = (\pi,0)$, which supports their reliability. Again, the DΓA prediction (here, a metallic self-energy with a visible momentum differentiation) agrees well with the final BSS-QMC results [black circles in Fig. 4(c)].

At the elevated temperature $T = 1/40$, the finite-size bias affects the raw BSS-QMC results even more drastically, as seen in Fig. 5: at both $\mathbf{k}$ points, the smallest systems (8×8, red downward triangles) have clearly insulating character, while DΓA (dash-double-dotted line) yields a metallic solution,

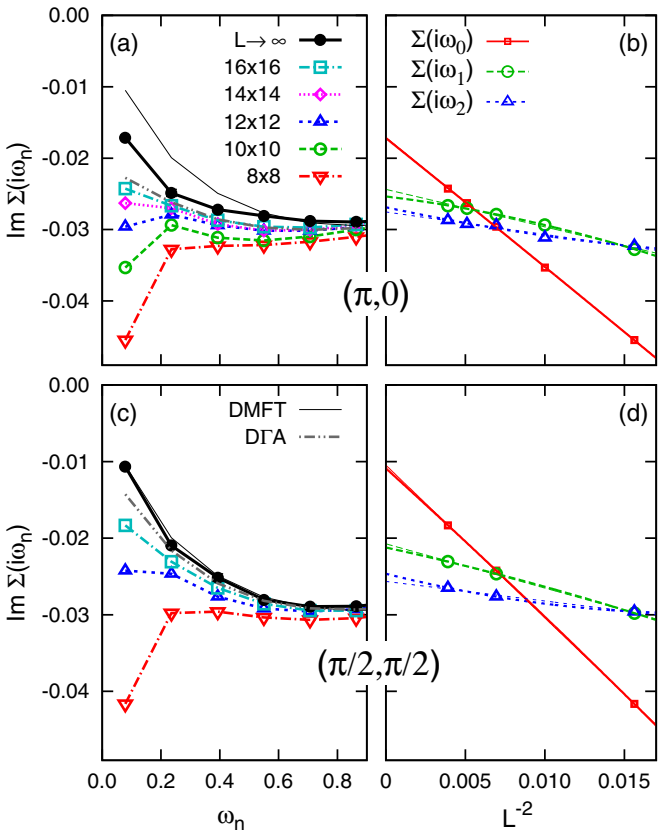

FIG. 5. (Color online) Self-energy on the imaginary axis at $U = 0.5$, $\beta = 40$, analogous to Fig. 4.

just like (paramagnetic) DMFT (thin gray line). However, the 16×16 system (squares) is already large enough to show significant metallic tendencies. Even more importantly, Figs. 5(b) and 5(d) demonstrate that the dependency of the raw BSS-QMC data on L^{-2} is very regular and almost linear again (even across the FS-induced metal-insulator crossover), so that the extrapolation $L^{-2} \to 0$ is still reliable, with even smaller resulting error bars than at $T = 1/100$. Interestingly, the final BSS-QMC results at $\mathbf{k} = (\pi/2,\pi/2)$ [black circles in Fig. 5(c)] agree with DMFT within error bars; only at $\mathbf{k} = (\pi,0)$ do nonlocal antiferromagnetic correlations induce a significantly more insulating character.

[1] N. F. Mott, Rev. Mod. Phys. **40**, 677 (1968); *Metal-Insulator Transitions* (Taylor and Francis, London, 1990); F. Gebhard, *The Mott Metal-Insulator Transition* (Springer, Berlin, 1997).

[2] J. Hubbard, Proc. R. Soc. London, Ser. A **276**, 238 (1963); M. C. Gutzwiller, Phys. Rev. Lett. **10**, 159 (1963); J. Kanamori, Prog. Theor. Phys. **30**, 275 (1963).

[3] F. Essler, H. Frahm, F. Göhmann, A. Klümper, and V. Korepin, *The One-Dimensional Hubbard Model* (Cambridge University Press, Cambridge, 2010).

[4] K. Kawakami, T. Usuki, and A. Okiji, Phys. Lett. A **137**, 287 (1989).

[5] T. D. Stanescu and P. Phillips, Phys. Rev. B **64**, 235117 (2001).

[6] A. Georges, G. Kotliar, W. Krauth, and M. Rozenberg, Rev. Mod. Phys. **68**, 13 (1996).

[7] W. Metzner and D. Vollhardt, Phys. Rev. Lett. **62**, 324 (1989).

[8] A. Georges and G. Kotliar, Phys. Rev. B **45**, 6479 (1992).

[9] P. R. C. Kent, M. Jarrell, T. A. Maier, and Th. Pruschke, Phys. Rev. B **72**, 060411(R) (2005).

[10] R. Staudt, M. Dzierzawa, and A. Muramatsu, Eur. Phys. J. B **17**, 411 (2000); E. Kozik, E. Burovski, V. W. Scarola, and M. Troyer, Phys. Rev. B **87**, 205102 (2013).

[11] G. Rohringer, A. Toschi, A. Katanin, and K. Held, Phys. Rev. Lett. **107**, 256402 (2011).

[12] S. Fuchs, E. Gull, L. Pollet, E. Burovski, E. Kozik, T. Pruschke, and M. Troyer, Phys. Rev. Lett. **106**, 030401 (2011).

[13] E. Gull, P. Staar, S. Fuchs, P. Nukala, M. S. Summers, T. Pruschke, T. C. Schulthess, and T. Maier, Phys. Rev. B **83**, 075122 (2011).

[14] P. Hansmann, A. Toschi, G. Sangiovanni, T. Saha-Dasgupta, S. Lupi, M. Marsi, and K. Held, Phys. Status Solidi B **250**, 1251 (2013).

[15] C. Castellani, C. Di Castro, D. Feinberg, and J. Ranninger, Phys. Rev. Lett. **43**, 1957 (1979).

[16] M. Vekic and S. R. White, Phys. Rev. B **47**, 1160 (1993).

[17] F. Mancini, Eur. Phys. Lett. **50**, 229 (2000).

[18] R. Eder, C. Gröber, M. C. Zacher, and W. Hanke, in *Open Problems in Strongly Correlated Electron Systems*, edited by J. Bonca *et al.*, NATO Science Series, Series II, Mathematics, Physics, and Cchemistry Vol. 15, (Kluwer Academic, Dordrecht, 2001), Part I, pp. 23–31.

[19] A. Avella, F. Mancini, and R. Münzner, Phys. Rev. B **63**, 245117 (2001).

[20] F. Mancini and A. Avella, Adv. Phys. **53**, 537 (2007).

[21] J. M. Vilk and A.-M. S. Tremblay, Eur. Phys. Lett. **33**, 159 (1996); J. Phys. I **7**, 1309 (1997).

[22] S. Moukouri, S. Allen, F. Lemay, B. Kyung, D. Poulin, Y. M. Vilk, and A.-M. S. Tremblay, Phys. Rev. B **61**, 7887 (2000).

[23] A.-M. Darè, L. Raymond, G. Albinet, and A.-M. S. Tremblay, Phys. Rev. B **76**, 064402 (2007).

[24] Due to the strong-coupling nature of correlations in two dimensions at low T the applicability of more conventional perturbative schemes is typically very limited. Specifically, the fluctuation exchange approximation (FLEX) is unable to predict a pseudogap phase in the 2D Hubbard model in the sense of momentum differentiation (see, e.g., [21]). The one-loop functional renormalization group/parquet approximations (PA) do not satisfy the Mermin-Wagner theorem (see [59]) and find long-range antiferromagnetic order at finite T.

[25] P. W. Anderson, *The Theory of Superconductivity in the High-T_C Cuprates*, Princeton Series in Physics (Princeton University Press, Princeton, NJ, 1997).

[26] H. Park, K. Haule, and G. Kotliar, Phys. Rev. Lett. **101**, 186403 (2008).

[27] T. A. Maier, M. Jarrell, T. Pruschke, and M. H. Hettler, Rev. Mod. Phys. **77**, 1027 (2005).

[28] Early pioneering DCA results [60] indicating a reduction of U_c have been questioned [61, 53] and show imprecise estimates of U_c as well as no coexistence region. These have been superseded by more recent cluster-DMFT [26] and DCA analyses [62, 63].

[29] A. N. Rubtsov, M. I. Katsnelson, and A. I. Lichtenstein, Phys. Rev. B **77**, 033101 (2008); S. Brener, H. Hafermann, A. N. Rubtsov, M. I. Katsnelson, and A. I. Lichtenstein, *ibid.* **77**, 195105 (2008).

[30] H. Hafermann, Ph.D. thesis, University of Hamburg, 2009.

[31] M. Potthoff, M. Aichhorn, and C. Dahnken, Phys. Rev. Lett. **91**, 206402 (2003).

[32] A. Toschi, A. A. Katanin, and K. Held, Phys. Rev. B **75**, 045118 (2007); K. Held, A. A. Katanin, and A. Toschi, Prog. Theor. Phys. Suppl. **176**, 117 (2008).

[33] R. Blankenbecler, D. J. Scalapino, and R. L. Sugar, Phys. Rev. D **24**, 2278 (1981).

[34] F. F. Assaad and H. G. Evertz, in *Computational Many Particle Physics*, edited by H. Fehske, R. Schneider, and A. Weiße, Lecture Notes in Physics Vol. 739 (Springer, Berlin, 2008), p. 277.

[35] M. Golor, T. Reckling, L. Classen, M. M. Scherer, and S. Wessel, Phys. Rev. B **90**, 195131 (2014).

[36] N. Blümer, Phys. Rev. B **76**, 205120 (2007).

[37] D. Rost, E. V. Gorelik, F. Assaad, and N. Blümer, Phys. Rev. B **86**, 155109 (2012).

[38] M. Balzer, B. Kyung, D. Senechal, A.-M. S. Tremblay, and M. Potthoff, Europhys. Lett. **85**, 17002 (2009).

[39] N. Blümer, Ph.D. thesis, University of Augsburg, 2002.

[40] A. A. Katanin, A. Toschi, and K. Held, Phys. Rev. B **80**, 075104 (2009).

[41] N. D. Mermin and H. Wagner, Phys. Rev. Lett. **17**, 1133 (1966).

[42] G. Rohringer, A. Toschi, H. Hafermann, K. Held, V. I. Anisimov, and A. A. Katanin, Phys. Rev. B **88**, 115112 (2013).

[43] C. Taranto, S. Andergassen, J. Bauer, K. Held, A. Katanin, W. Metzner, G. Rohringer, and A. Toschi, Phys. Rev. Lett. **112**, 196402 (2014); N. Wentzell, C. Taranto, A. Katanin, A. Toschi, and S. Andergassen, Phys. Rev. B **91**, 045120 (2015).

[44] G. Rohringer, A. Valli, and A. Toschi, Phys. Rev. B **86**, 125114 (2012).

[45] T. Schäfer, G. Rohringer, O. Gunnarsson, S. Ciuchi, G. Sangiovanni, and A. Toschi, Phys. Rev. Lett. **110**, 246405 (2013).

[46] E. Gull, M. Ferrero, O. Parcollet, A. Georges, and A. J. Millis, Phys. Rev. B **82**, 155101 (2010).

[47] A. Altland and B. Simons, *Condensed Matter Field Theory* (Cambridge University Press, Cambridge, 2006).

[48] J. P. F. Le Blanc and E. Gull, Phys. Rev. B **88**, 155108 (2013).

[49] S. R. White, D. J. Scalapino, R. L. Sugar, E. Y. Loh, J. E. Gubernatis, and R. T. Scalettar, Phys. Rev. B **40**, 506 (1989).

[50] T. Baier, E. Bick, and C. Wetterich, Phys. Rev. B **70**, 125111 (2004).

[51] K. Borejsza and N. Dupuis, Europhys. Lett. **63**, 722 (2003); Phys. Rev. B **69**, 085119 (2004).

[52] E. M. Motoyama, G. Yu, I. M. Vishik, O. P. Vajk, P. K. Mang, and M. Graven, Nature (London) **445**, 186 (2007).

[53] E. Gull, P. Werner, X. Wang, M. Troyer, and A. J. Millis, Eur. Phys. Lett. **84**, 37009 (2008).

[54] C. Taranto, G. Sangiovanni, K. Held, M. Capone, A. Georges, and A. Toschi, Phys. Rev. B **85**, 085124 (2012); A. Toschi, M. Capone, and C. Castellani, *ibid.* **72**, 235118 (2005).

[55] E. Gull and A. J. Millis, Phys. Rev. B **86**, 241106(R) (2012).

[56] P. Korbel, W. Wójcik, A. Klejnberg, J. Spałek, M. Acquarone, and M. Lavagna, Eur. Phys. J. B **32**, 315 (2003).

[57] E. V. Gorelik and N. Blümer, Phys. Rev. A **80**, 051602(R) (2009).

[58] N. Blümer and E. V. Gorelik, Phys. Rev. B **87**, 085115 (2013).

[59] A. T. Zheleznyak, V. M. Yakovenko, and I. E. Dzyaloshinskii, Phys. Rev. B **55**, 3200 (1997).

[60] S. Moukouri and M. Jarrell, Phys. Rev. Lett. **87**, 167010 (2001).

[61] B. Kyung, J. S. Landry, D. Poulin, and A.-M. S. Tremblay, Phys. Rev. Lett. **90**, 099702 (2003).

[62] J. Merino and O. Gunnarsson, Phys. Rev. B **89**, 245130 (2014).

[63] E. Gull, O. Parcollet, and A. J. Millis, Phys. Rev. Lett. **110**, 216405 (2013).